Journal of Materials Chemistry A

PAPER

View Article Online
View Journal | View Issue

Cite this: J. Mater. Chem. A, 2014, 2, 16498

Molecular dynamics investigation of carbon nanotube junctions in non-aqueous solutions

K. Gkionis,[a] J. T. Obodo,[a] C. Cucinotta,[b] S. Sanvito[b] and U. Schwingenschlögl*[a]

Received 1st June 2014
Accepted 23rd July 2014

DOI: 10.1039/c4ta02760d

www.rsc.org/MaterialsA

The properties of liquids in a confined environment are known to differ from those in the bulk. Extending this knowledge to geometries defined by two metallic layers in contact with the ends of a carbon nanotube is important for describing a large class of nanodevices that operate in non-aqueous environments. Here we report a series of classical molecular dynamics simulations for gold-electrode junctions in acetone, cyclohexane and *N*,*N*-dimethylformamide solutions and analyze the structure and the dynamics of the solvents in different regions of the nanojunction. The presence of the nanotube has little effect on the ordering of the solvents along its axis, while in the transversal direction deviations are observed. Importantly, the orientational dynamics of the solvents at the electrode–nanotube interface differ dramatically from that found when only the electrodes are present.

Introduction

Nanoscale devices have attracted intense interest among researchers over the past decades, due to their wide range of applications. Biotechnology is an example of a field where advances in nanotechnology can be highly beneficial. Applications range from drug delivery[1] and DNA sequencing[2] to tissue engineering[3] and sensing devices.[4,5] The latter technological area often employs carbon nanotubes (CNTs) as active element for the detection of the species of interest. In fact, single or multi-walled nanotube field-effect transistors are often used in biosensors, in which the nanotube is mounted between electrodes and the analyte is detected by its effect on the electrical response of the CNT itself.

Since species of biological interest typically appear in an aqueous environment, biosensors are aimed at functioning in wet conditions, although devices functioning in non-aqueous solutions are also of interest. For example, Grüner and co-workers have investigated the interactions of different benzene derivatives with CNTs in non-aqueous media, such as cyclohexane, revealing a linear relationship between the gate voltage shifts and the Hammett constants of the benzene substituents.[6] The same study has compared the *I*–*V* characteristics of the CNT field-effect transistors immersed in non-aqueous media and in air. Along the same lines, the dependence of the response on the size of the aromatic compounds and the detection of amine derivatives has been investigated,[7] both being of interest in the context of hydrocarbon fuels.

The presence of a medium, whether aqueous or non-aqueous, affects the electrical response of a device and thus has to be taken into account in a measurement. The electrodes of a sensor act as confining walls for the solvents, which in turn exhibit different properties than those in the absence of confinement. Hence, knowledge of the behavior of confined solvents in the presence of CNTs in a typical device geometry is important for understanding the function of the device itself. Spectroscopy can be used for investigating the orientations of solvents and molecules in metal–CNT junctions. Specifically, the orientation of the molecules has been addressed by Raman spectroscopy and the orientational dynamics have been explored by second harmonic generation measurements.[8,9] Nowadays sufficiently long molecular dynamics (MD) simulations of large systems are feasible to complement such experiments by providing details at the molecular level.

In general, computational modeling is a valuable tool for studying material properties. For example, MD simulations are routinely employed to investigate structural and dynamical aspects of confined liquids[10,11] and nanotubes in wet conditions.[12] Similarly, *ab initio* calculations provide the electronic structure of matter and are useful in predicting transport properties in nanojunctions. Importantly, a combination of MD and *ab initio* calculations allows one to evaluate the transport properties of nano-devices in wet conditions, by taking into account the dynamical behavior of the solvents in an averaged manner.[13]

Although various MD studies of confined liquids and nanotubes have been reported in the literature, to the best of our knowledge work on nanojunctions in solution is still lacking. Previously, the Gao, Luedtke and Landman approach[14] has been employed for the study of confined liquids and it has been demonstrated that such a setup is useful for analyzing nanotube–electrode nanojunctions.[15] In particular, the efficiency of

[a]KAUST, PSE Division, Thuwal 23955-6900, Kingdom of Saudi Arabia. E-mail: udo.schwingenschlogl@kaust.edu.sa; Tel: +966 544700080
[b]School of Physics and CRANN, Trinity College, Dublin 2, Ireland

the procedure for estimating the number of molecules within the junction in the presence of a nanotube has been stressed. In the present study we employ the same approach to investigate the structure and the dynamics of non-aqueous solvents, namely acetone, cyclohexane and *N*,*N*-dimethylformamide (DMF) in Au/CNT/Au junctions. Note that all the three solvents are of potential interest in the field of hydrocarbon fuels.[6,7]

Methods

Fig. 1 displays the three solvent molecules considered in this study, namely acetone, cyclohexane and DMF, while the geometry of the device investigated, along with the reference Cartesian axes, is shown in Fig. 2. This geometry is convenient for our device setup.[15] In fact the presence of the nanotube fixes the distance between the two electrodes and therefore the size of the cell in the direction of the nanotube, so that a barostat-type optimization is impossible. We use electrodes with periodic boundary conditions in the *x*-direction only to reduce the complexity of adjusting the solvent's density for a given pressure by varying the volume.[15] We now investigate the structure and the dynamics of Au/CNT/Au nanojunctions immersed in different liquid solvents. In particular the properties of the nanoconfined solvents are compared to those obtained under the simple confinement provided by two Au electrodes only, *i.e.*, in the absence of the nanotube. The anisotropic arrangement of the nanotube in our model enables us to gain insight into the effect of different confinement geometries on the behavior of the solvents.

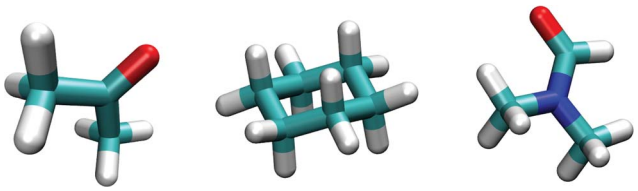

Fig. 1 The three solvents considered in this work: from left to right: acetone, cyclohexane and DMF.

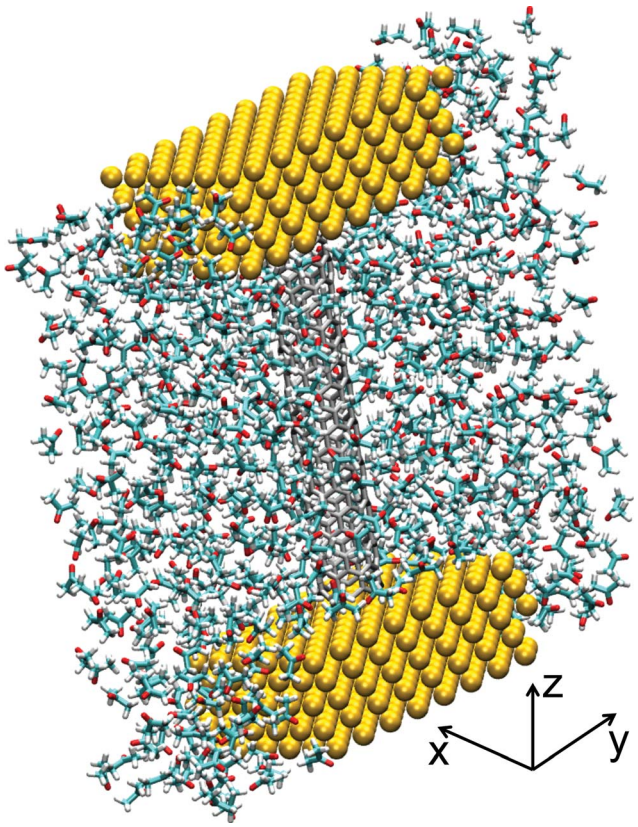

Fig. 2 The geometry of the devices simulated and the reference Cartesian axes. Au atoms are shown as yellow spheres, C atoms as grey capped sticks.

The electrodes expose their Au(111) surfaces and have dimensions of $1.6 \times 3.9 \times 0.9$ nm^3, consisting of 5 layers of gold with 96 atoms per layer. This results in a total of 960 gold atoms. The CNT is 3.7 nm long, it has a diameter of 0.6 nm, and comprises 288 carbon atoms. The distance between the CNT and each of the electrodes is kept fixed at 0.21 nm (a value obtained with *ab initio* optimization[16]). Thus the surfaces of the electrodes are separated by 4.15 nm. The solvent molecules partially surround the electrodes, as shown in Fig. 2, thus only a portion of the solvent is confined between the electrodes and the molecules are also in contact with the electrodes' sides. The number of solvent molecules used in our simulations is respectively 600 for acetone, 300 for cyclohexane and 500 for DMF. Moreover, the simulation box in the *xz*-plane spans an area of 1.7×6.3 nm^2 in all cases, with the *y*-dimension being readjusted by means of an isobaric simulation (see below for further details). The dynamics of the structural morphology are studied at zero bias. Finite bias might slightly affect the alignment (polarization) of the molecules of the solvent and thus the electrical response.

All calculations are performed with the NAMD software[17] and the implemented CHARMM force-field.[18] CHARMM parameters are employed for the description of cyclohexane and the aromatic carbon atoms of the CNT, while for DMF and acetone we use the CHARMM General Force Field parameterization.[19] Finally, gold is described by the parameterization of Heinz and co-workers.[20] Gold and CNT atoms are neutral and kept fixed at their ideal positions during all the simulations. Bonds involving hydrogen atoms are kept rigid for all the solvents and the cyclohexane is kept rigid in its most stable chair conformation.

Non-bonding interactions between heteroatoms are described by the Lorentz and Berthelot mixing rules, *i.e.*, by employing the arithmetic mean for the contact distance, $r_{\mathrm{min},ij}$, and the geometric mean for the interaction energy, ε_{ij}, of the Lennard-Jones potential. For atoms separated by more than 1.0 nm they smoothly vanish beyond 1.2 nm. For interatomic distances larger than this threshold the non-bonding interactions are included as a correction.[21] Long-range Coulomb interactions are described by using the particle-mesh Ewald method[22] for computing the Ewald summation.[23] Electrostatic interactions are evaluated every 4 fs, while the timestep of the simulation is 2 fs.

All systems are initially treated by energy minimization for 5000 steps in order to eliminate steric clashes. Subsequently, the systems are gradually heated to the target temperature of 300 K at a rate of 0.5 K every 200 fs by using the velocity reassignment method. After these initial steps all the systems are

Table 1 Average length of the systems in the y-direction after NPT equilibration

System	y (nm)
Acetone	7.9
Acetone, CNT	8.2
Cyclohexane	6.2
Cyclohexane, CNT	6.5
DMF	7.1
DMF, CNT	7.4

simulated in the isothermal–isobaric ensemble (NPT) at 1 atm for 160 ns, during which the xz area is kept constant and only the y-dimension is allowed to readjust. The pressure is kept constant by the Nosé–Hoover method[24] and the piston fluctuation control[25] with a piston period of 400 fs, decay of 200 fs and temperature of 300 K. The equilibrium size of every cell along the y-direction is obtained by averaging out the values of the NPT simulation (see Table 1). This scheme for optimizing the cell volume allows us to control the density of the system.

Subsequently, a NVT simulation is performed for 2 ns with the volume defined by the initial x- and z-dimensions (kept constant) and the average y-dimensions listed in Table 1. For both the NPT and NVT simulations the temperature is controlled by a local Langevin thermostat with a Langevin coefficient of 5 ps^{-1} applied to all atoms. Once the systems are equilibrated the thermostat is removed and the microcanonical ensemble (NVE) is employed for 2 ns, during which the trajectory is recorded every 10 fs for analysis.

Results

Fig. 3 displays the obtained profiles along the z-axis for the region in which the solvent molecules are confined between the gold electrodes. An advantage of our model is that the two surfaces of the metal electrodes are equivalent, thus that the density profiles are symmetric with respect to the median plane of the device. As a consequence we can average over two half cells, decreasing the statistical error in the computation of the density profiles.

In all cases we obtain typical profiles of confined liquids, with peaks of higher density next to the gold surfaces, which gradually disappear away from the surface. An exception is the case of cyclohexane, which exhibits a more structured density profile along the z-axis, as predicted before.[26,27] The density peaks due to the proximity to the surfaces occur at distances of 3.3 Å for all solvents and irrespective of whether or not the CNT is present. For acetone and DMF a second peak appears respectively at 7.0 and 6.6 Å from the surface, and finally near the middle of the junction (beyond 17 Å in Fig. 3) the density eventually tends to a constant value. In this region the average densities of acetone, cyclohexane and DMF are 0.809 g cm^{-3} (0.03), 0.740 g cm^{-3} (0.32) and 0.994 g cm^{-3} (0.04), respectively (in brackets we report the standard deviations). These values are very close to the reported values[28] of 0.791, 0.779 and 0.944 g cm^{-3}. Cyclohexane in this region exhibits the mentioned oscillations, ranging from 0.330 to 1.199 g cm^{-3} both when the CNT is present or not.

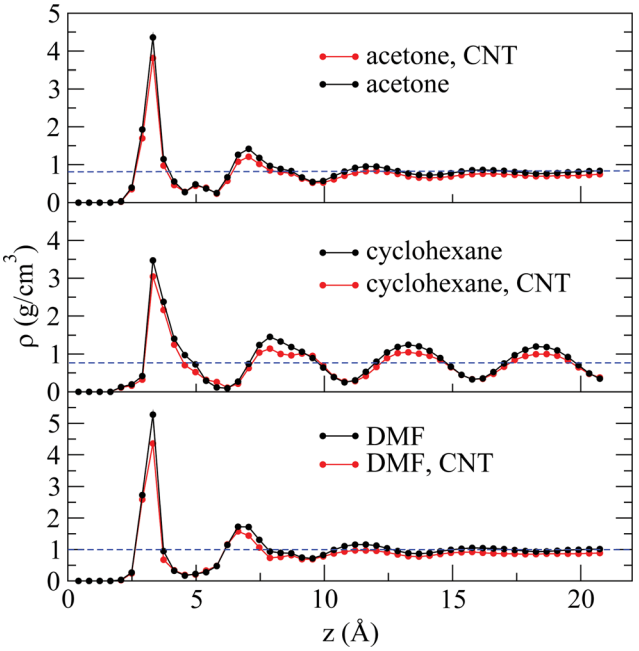

Fig. 3 Density profiles along the z-axis for the entire system. Horizontal blue dashed lines represent the calculated average density in the bulk. The Au surface boundary is at $x = 0$.

In the same region the density of a solvent in the presence of the CNT averages to a lower value than that obtained in the absence of the CNT, namely 0.721, 0.665 and 0.876 g cm^{-3} for acetone, cyclohexane and DMF, respectively. This behavior is due to the volume occupied by the nanotube and it is not an indication that the actual density drops. In fact the ratios of the average densities calculated either without and with nanotubes for each solvent are almost identical (acetone: 1.12, DMF: 1.13, cyclohexane: 1.11). The volume of the CNT is the same in all cases and the minor discrepancies observed are attributed to subtle differences among the solvents, related to the additional volume excluded by the nanotube–solvent non-bonding interactions.

We further evaluate the density profiles along the y-axis (Fig. 4, left). In this case, we consider a slab that is only 5 Å thick along the z-direction (blue lines labeled as "middle" in Fig. 4). The slab is taken in the central region of the junction in order to maintain the distance to each surface as large as possible (approximately 18 Å). As expected, in the absence of the CNT the densities for this region remain practically constant, as if there was only a bulk solvent (blue dashed line in Fig. 4). We obtain 0.802 (0.01), 0.780 (0.04) and 0.982 (0.04) g cm^{-3} for acetone, cyclohexane and DMF, respectively. The presence of the CNT perturbs the profiles and peaks are obtained near the CNT, indicating that the solvents assume structures similar to solvation layers. In all the cases the density is increased at a distance ranging between 3.3 Å and 3.4 Å from the CNT, in a rather similar way to the first peak observed for the gold surface. A second, although rather small, peak is observed at larger distances (8 Å to 9 Å) from the CNT for all the solvents, *i.e.*, at a significantly larger distance than the second peaks computed for Au.

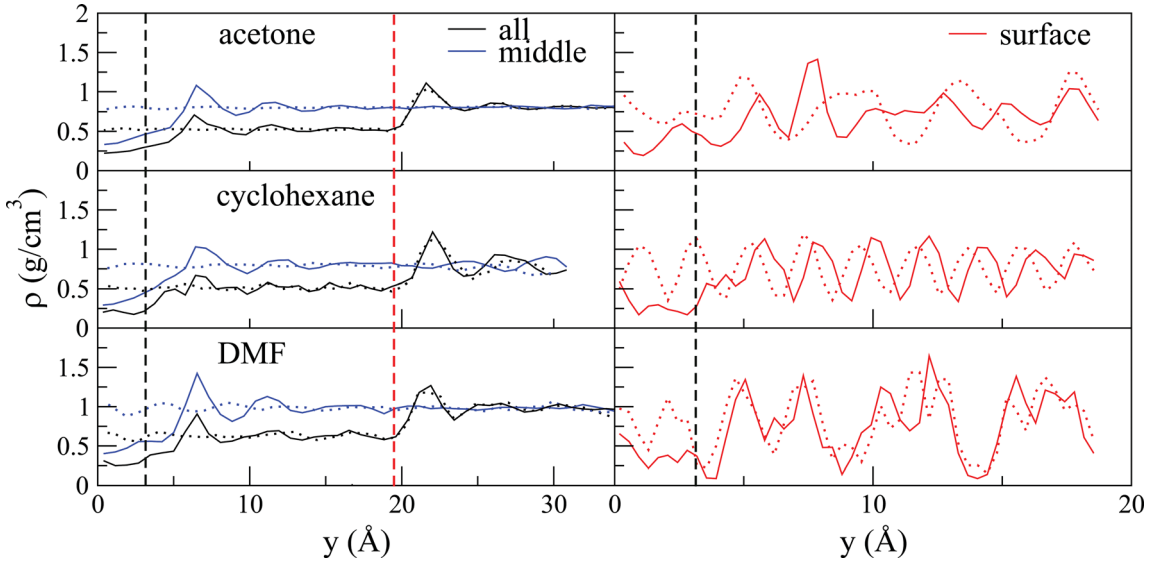

Fig. 4 Left: the density profiles along the *y*-axis for the entire system (all) and for a slice cut in the middle of the junction (middle). Right: density profiles along the *y*-axis at the electrode surface. In all the graphs continuous and dashed lines correspond respectively to the presence and the absence of the CNT. Vertical dashed green and red lines indicate the boundary along the *y*-axis of the CNT and the electrode, respectively.

In order to study the extent of the perturbation introduced to the density profiles by the finite nature of the electrodes along the *y*-axis (the edge is represented by the red line in Fig. 4), we plot the density profile along this direction considering the entire system (black lines in Fig. 4, left). While the general trend of the profile is reproduced, in the confined region the density plots are shifted to lower values. This is a direct effect arising from the larger volume. It is interesting to note that in the region within the electrodes (between the green and red dashed lines in Fig. 4) the average density is not strongly affected by the presence of the electrode edge. Instead, the edge perturbs the profiles in the region between 20 Å and 25 Å in Fig. 4, *i.e.* outside the confined region, where a peak is observed in all profiles. These peaks are similar to those observed near the Au(111) surface (see Fig. 3), but here they are due to the proximity of the solvents to the side of the electrode. In all cases, beyond this perturbation (distances longer than 25 Å) all profiles converge to approximately the same value. An exception is cyclohexane, for which all profiles are noisy and maintain averages between 0770 g cm^{-3} and 0.815 g cm^{-3}.

Another point of interest is the average density profile along the *y*-direction, measured over a slice that is adjacent to the surface. We consider a 5 Å-thick slice so that to roughly correspond to the solvent molecules that are enclosed within the first density peak along the *z*-axis (Fig. 3). In this case, the density of this first layer of solvent molecules next to the surface oscillates both when a CNT is present and when it is absent. The main difference between the two cases is the reduced density in the region occupied by the CNT. The oscillations are the result of the fact that the slice contains only the molecules adjacent (adsorbed) to the surface. Thus, the profile is largely affected by the intramolecular atomic arrangement of each solvent.

A third profile is evaluated for two equal-sized regions around the CNT, as schematically displayed in Fig. 5. These two profiles, presented in Fig. 6, are evaluated in order to determine the effect of different confinement geometries along the *x*-axis, since in our systems the periodic images of the CNT in the *x*-direction are much closer than those along the *y*-direction.

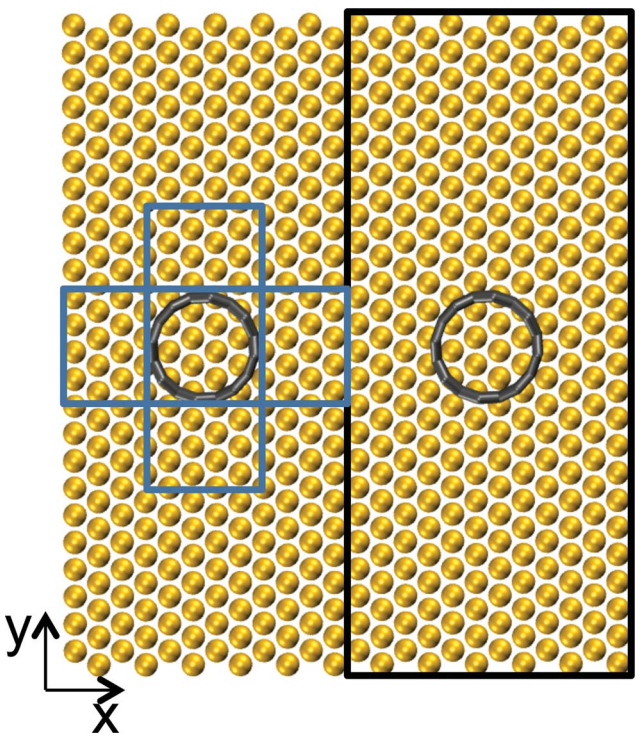

Fig. 5 Top view of the Au/CNT/Au device investigated. The blue rectangles on the left-hand side indicate the spatial regions around the CNT (ring) used to construct the density profiles reported in Fig. 6. The black rectangle on the right-hand side highlights the periodic image along the *x*-direction.

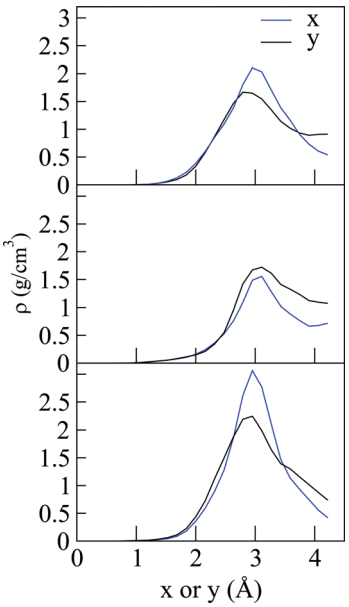

Fig. 6 Density profiles calculated for two narrow regions cut around the CNT respectively along the *x*- and *y*-direction (top: acetone, middle: cyclohexane, bottom: DMF). The $x = 0$ position corresponds to the boundary of the nanotube. The regions used for the calculations are shown in Fig. 5.

The peaks in the profiles due to the CNT confinement effect are found at the same position for both directions. However, a notable difference in the magnitude of the peaks is observed. In the cases of acetone and DMF the peak is more pronounced along the *x*-direction, due to the proximity of the periodic images, which acts as additional confinement and enhances the ordering of the solvents. However, this feature is not observed for cyclohexane, where the peaks along the *x*- and *y*-directions are practically identical. Such a difference is probably due to the less flexible geometry of cyclohexane as compared to acetone and DMF, which prevents a stronger ordering than that already induced for this system geometry.

While the density profiles examined above reflect the ordering due to the confinement, the formalism of the second order parameter can provide additional insights into whether there are deviations from a random arrangement of the molecules at or near the interfaces. The second order parameter is given by:

$$P_2(\cos\theta) = \frac{3}{2}\langle\cos^2(\theta)\rangle - \frac{1}{2} \quad (1)$$

where θ is the angle between an arbitrary vector along the solvent molecule and the *z*-axis. The squared cosine is averaged over 2500 snapshots of the trajectories. The molecular vectors are oriented along the C=O bond for acetone, along the bond between the C atom in the carbonyl group and N for DMF and along two opposite C atoms (all C atoms are equivalent) for cyclohexane. The possible most interesting values of P_2 are −0.5, 1.0 and 0.0, which correspond to perpendicular, parallel and random orientation of the molecular vector with respect to the *z*-axis, respectively.

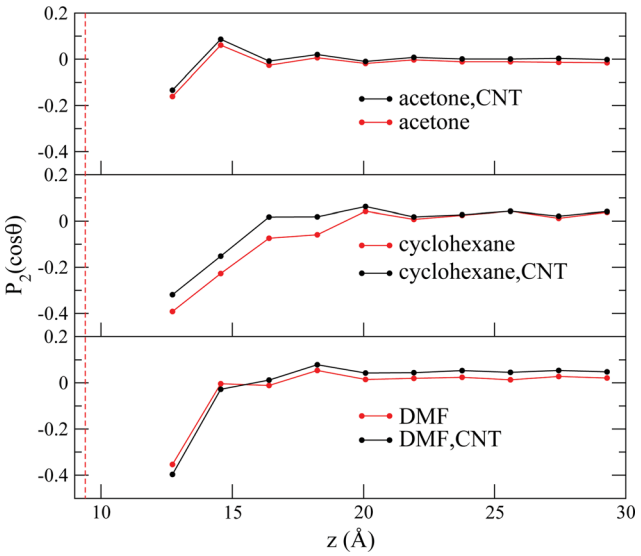

Fig. 7 Order parameter profile along the *z*-axis for molecules included in the confining region.

Fig. 7 shows the order parameter calculated by considering the trajectories only of molecules positioned within the confined region, *i.e.* those in between the two Au electrodes. Similar to the respective density profile along the *z*-axis, the pattern of the order parameter is maintained whether the CNT is present or not, for acetone and DMF, while cyclohexane does not follow the same trend. In all six curves of Fig. 7, P_2 attains negative values near the surfaces, with the most negative values for the adsorbed solvents on the surface, *i.e.*, the layer that corresponds to the density peaks. This indicates a tendency to an orientation parallel to the Au surface, which is more pronounced for DMF and cyclohexane.

The area where the angular orientation deviates from randomness roughly corresponds to the first minimum of the density along the *z*-axis (see Fig. 3). In cyclohexane this area tends to be larger and the onset of randomness is more gradual, which can be explained on the basis of the adopted orientations per layer. A snapshot of the cyclohexane system is shown in Fig. 8, where it is evident that molecules next to the surface have

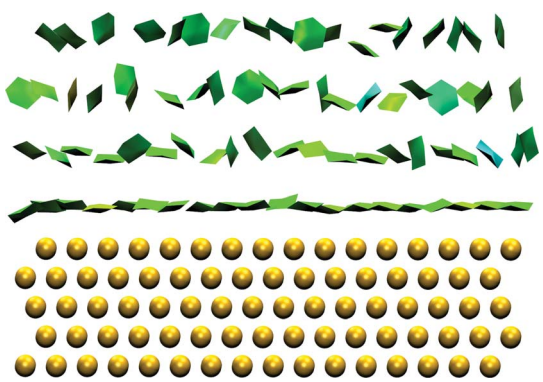

Fig. 8 Spatial distribution of cyclohexane molecules (shown as green planar chains for clarity) near the Au surface. Note that order is progressively lost as one moves away from the surface.

a clear tendency to orient themselves parallel to the surface. Molecules in the second layer from the surface still exhibit this tendency, although much weaker. The onset of randomness in the second layer and beyond is gradual.

Away from the surface and near the middle of the device P_2 becomes practically zero, indicating a random orientation of the solvent molecules. This is consistent with the observation that the average density resembles that of the unconfined solvent, while for cyclohexane minor oscillations of the order parameter are observed, reflecting the oscillatory behavior of the density.

Additional insights into the effects arising from the Au surface and the CNT on the solvent are gained by plotting P_2 against the y-axis for molecules that are found in the middle between the surfaces (confined region) or adjacent to each surface (Fig. 9). In this figure the full lines correspond to the device incorporating the CNT, while the dashed lines are for the two Au electrodes only. The values along the horizontal axis denote the distance from the central axis of the CNT ($y = 0$). Similar patterns are obtained for all the solvents when considering the molecules adjacent to the Au surface, whether the CNT is present or not. The order parameter P_2 maintains a negative value up to approximately 22 Å away from the center of the CNT, where it then grows to almost or even above zero for additional 3–4 Å and finally converges to zero (beyond 25 Å). The region where P_2 is close to zero corresponds to the volume beyond the boundaries of the electrodes, where a random orientation of the molecules is to be expected. This fact is consistent with the density profile along the y-axis, see Fig. 4, where we obtain bulk values in this same region. In the confined region (below 20 Å) the order parameters are constantly negative, ranging from -0.2 for acetone to -0.45 for cyclohexane and DMF, as expected by the profile along the z-axis (Fig. 7). The slightly positive values in the region between 20 Å and 25 Å are due to the molecules that lie on the yz-sides of the electrodes. In this region density peaks are observed along the same direction. Hence, such an effect is absent when only the middle region is considered (blue lines). In this case P_2 is nearly zero all along the y-axis, indicating that away from the surfaces all solvents orient themselves randomly, consistent with the fact that the densities approach bulk values. Since the interaction between the CNT and solvent does hardly depend on the surface curvature, the above results are expected to apply also to CNTs of larger diameter.

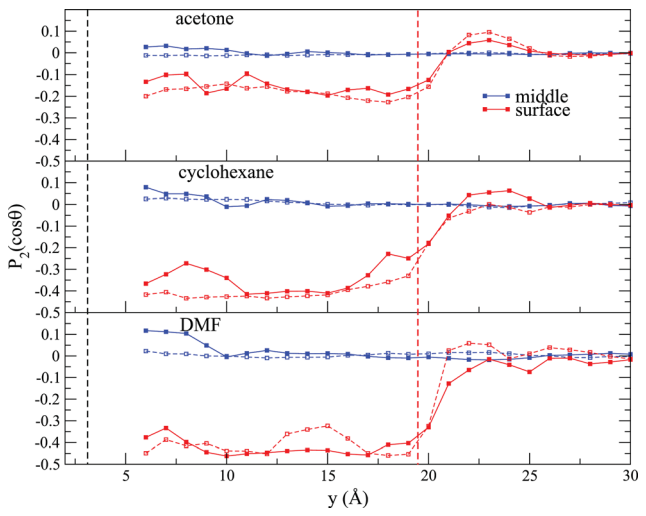

Fig. 9 Second order parameter $P_2(\cos(\theta))$ profiles along the y-axis for molecules in the middle between the surfaces (middle) and for molecules adjacent to the surfaces (surface). Continuous lines correspond to the presence of the CNT, dashed lines to its absence. Vertical green and red dashed lines indicate the boundaries of the CNT and Au surface, respectively.

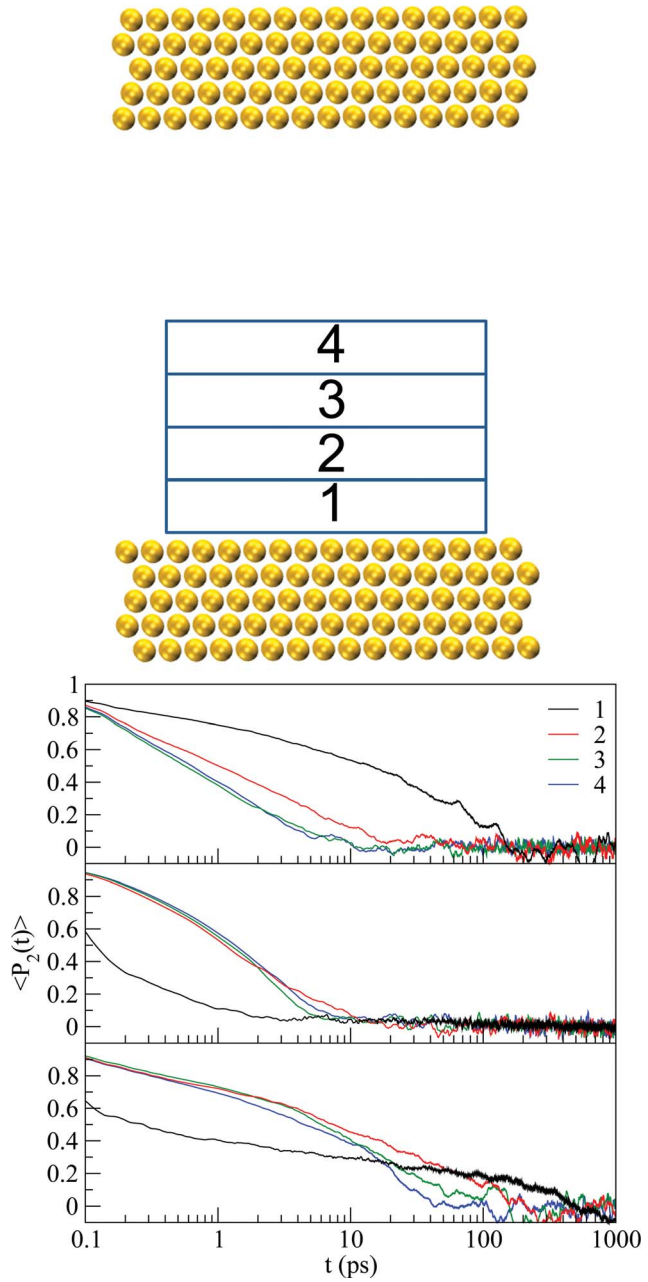

Fig. 10 Autocorrelation function for the order parameter $P_2(t)$ as a function of time: device not incorporating the CNT. From top to bottom we present results for acetone, cyclohexane and DMF. The numbers label the regions used in the calculation, which are displayed in the top panel.

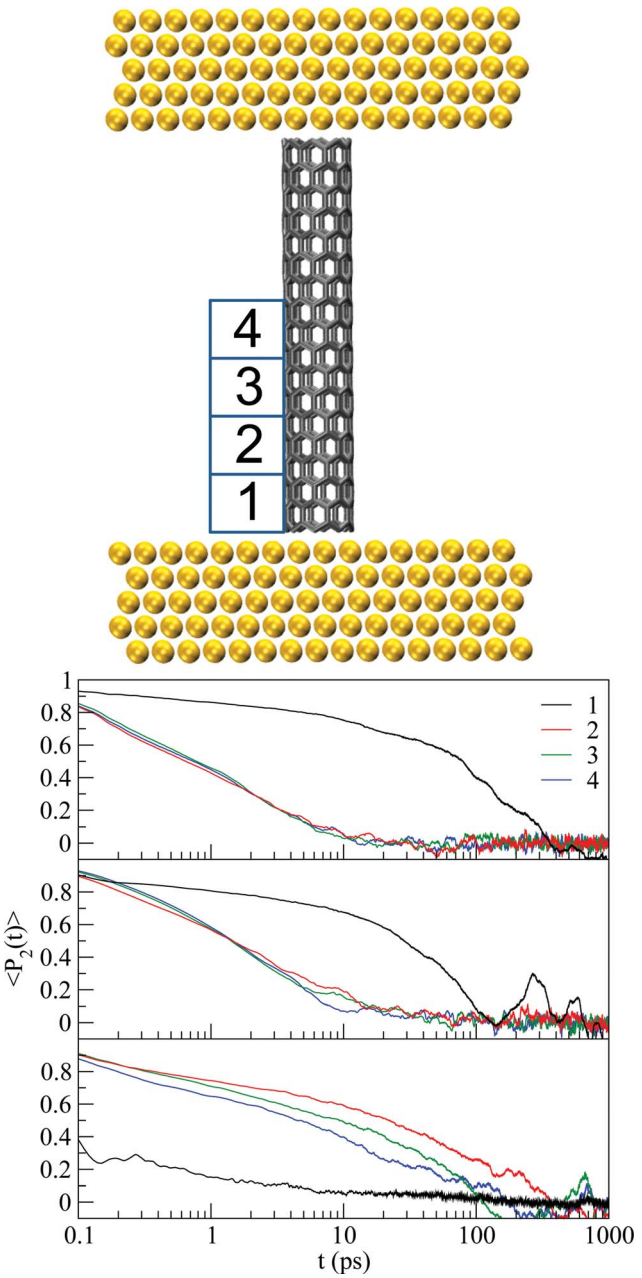

Fig. 11 Autocorrelation function for the order parameter $P_2(t)$ as a function of time: device incorporating the CNT and measurement regions close to the CNT. From top to bottom we present results for acetone, cyclohexane and DMF. The numbers label the regions used in the calculation, which are displayed in the top panel.

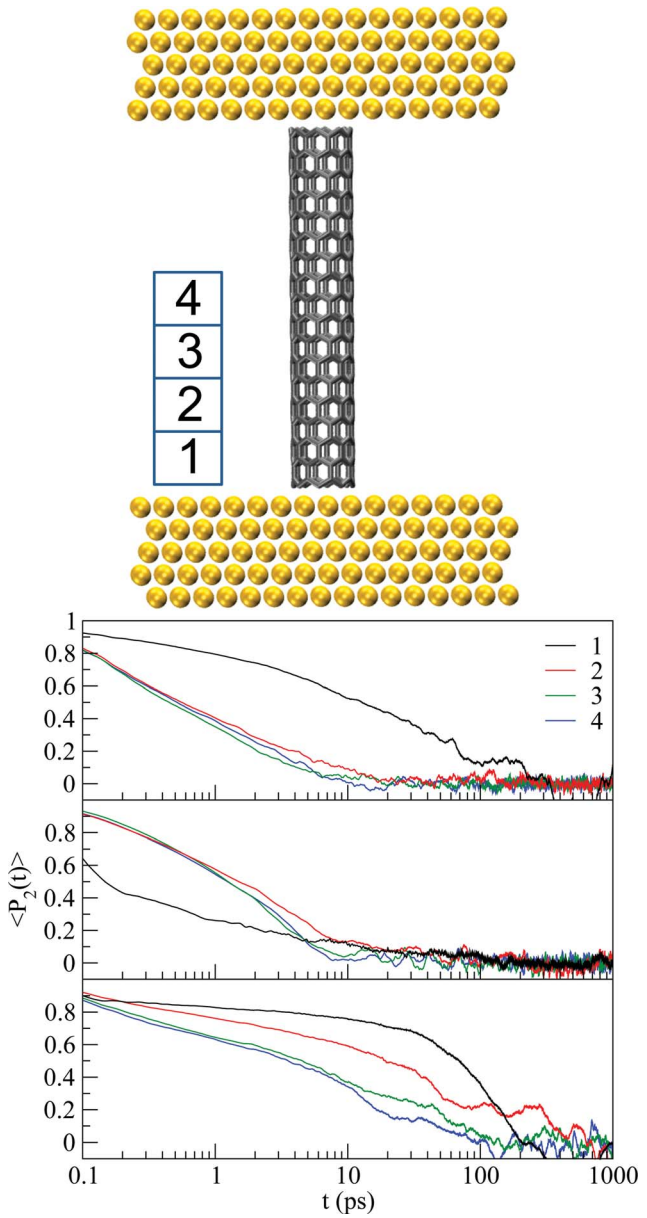

Fig. 12 Autocorrelation function for the order parameter $P_2(t)$ as a function of time: device incorporating the CNT and measurement regions far from the CNT. From top to bottom we present results for acetone, cyclohexane and DMF. The number labels the regions used in the calculation, which are displayed in the top panel.

Both the density profiles and the order parameter analyzed so far provide useful information on the system ordering, but no insight into its dynamics. Thus, we next focus on the orientation dynamics of the solvent molecules as a function of their distance from the surface and from the nanotube. To this aim, we consider the autocorrelation times $\langle P_2(t)\rangle$ of the order parameter. The molecular vectors for the three solvents are those defined before when calculating $P_2(\cos\theta)$. A plot of the investigated region and the corresponding autocorrelation diagrams are displayed in Fig. 10–12. The actual regions considered have been chosen to correspond to each solvent's density profile. We expect that the autocorrelation times for the system without the CNT (Fig. 10) and far away from the CNT (Fig. 12) are similar. In particular, longer autocorrelation times should be observed for region 1 (see Fig. 10–12), as it has been shown for the case of benzene confined between Au(111) surfaces.[11]

Longer autocorrelation times for region 1 are evident for all solvents (around 150–200 ps, 100 ps and 400–500 ps for acetone, cyclohexane and DMF, respectively) when no CNT is present (Fig. 10). For acetone and cyclohexane we find similar trends in Fig. 12, as expected, although longer autocorrelation times are

observed (around 100 ps). This is due to the fact that the volume of region 1 in Fig. 12 is smaller than that in Fig. 10. The respective region next to the CNT (Fig. 11) yields significantly longer autocorrelation times for cyclohexane (above 600 ps) and slightly longer for acetone (above 300 ps), since the molecules in region 1 adjacent to the nanotube are under the influence of the Au surface as well as the CNT, resulting in a slower reorientation. For DMF the correspondence between Fig. 10 and 12 is not as evident: in the latter case the curve seems to reach zero more rapidly than when the CNT is absent, a trend opposite to that for acetone and cyclohexane. However, it must be noted that while in most cases the curves oscillate around zero at long times, in Fig. 12 the negative values are more pronounced. Taking this negative correlation into account the de-correlation time is close to 1 ns, consistent with the increase observed for the other two solvents. On the other hand, shorter autocorrelation times are observed for DMF in the respective region next to the CNT (Fig. 11), in contrast to acetone and cyclohexane.

Concerning layers 2 to 4, no clear trend is observed. There is a tendency for layer 2 to yield longer autocorrelation times than layers 3 and 4 when the CNT is absent (Fig. 10) for all solvents, while this situation becomes more complex with the CNT. This behavior is connected with the observed density profiles for acetone and cyclohexane, which show that beyond the second peak any structure practically disappears (see Fig. 3). Therefore, no clearly distinctive behavior exists for layers beyond region 2 for these solvents.

For cyclohexane, the autocorrelation times are systematically shorter than for the other solvents, despite the fact that it has the most structured density profile under confinement. This is due to the fact that the interactions among cyclohexane molecules are different from those among acetone or DMF molecules. The latter two can form stable intermolecular hydrogen bonds at different relative orientations, as is known from their dimers.[29,30] Cyclohexane lacks the ability of H-bond formation in homo-dimers. More importantly, a stable dimer can be formed at a specific relative orientation of the consisting monomers, while other arrangements are disfavored.[31] These facts give rise to the shorter autocorrelation times observed for cyclohexane in the present study. The relative ease at which the solvent molecule interacts with its species can also explain the different behavior observed between cyclohexane and benzene under confinement: benzene molecules are similarly structured, but the molecules of the first layer next to the surface do not fully relax[11] in contrast to cyclohexane. However, benzene molecules, being the aromatic hydrocarbon equivalent of cyclohexane, develop π-stacking interactions both in stacked and parallel displaced geometries, which, similar to the ability of H-bonding discussed above, is not the case for cyclohexane. Finally, for cyclohexane in the absence of the CNT (Fig. 10) the regions 2 to 4 show a similar behavior, with autocorrelation times ranging between 20 and 30 ps. Again, this agrees with the data obtained away from the CNT (Fig. 12) and our working hypothesis. In particular, the autocorrelation times are of slightly larger magnitude, as observed for the first layer, and a clear trend between the layers is not evident. In the region adjacent to both the Au surface and the CNT (region 1, Fig. 11) the curve is noisy but a considerable increase is observed up to about 500 ps. Overall, there is systematic agreement between the different data.

Conclusions

A series of classical MD calculations has been presented aiming at understanding the structural behavior of selected solvents (acetone, cyclohexane and DMF) in a Au/CNT/Au nanojunction. Density profiles reveal the characteristic ordering known for confined liquids. In particular, a higher density is observed in proximity to the gold surfaces. The density peaks gradually vanish away from the gold surface for acetone and DMF, while cyclohexane maintains the ordering. Away from the gold surfaces and outside the confined region the average density of all solvents is found to be very close to the bulk value. The profiles parallel to the CNT are unaltered in the presence of the CNT, while in the perpendicular direction peaks are observed near the CNT. These latter are found to be of lower magnitude than those at the gold surfaces, since the CNT-solvent interaction is weaker.

Additional information on the ordering is obtained by evaluating the order parameter P_2 as a function of the distance from the electrode surface or the CNT. Near the electrodes a deviation from a complete orientational randomness is observed for all solvents, as the molecules tend to orient themselves parallel to the gold surface. Otherwise a random orientation is observed, consistent with the fact that the density approaches its ideal value. Moreover, the P_2 profiles are maintained in the presence of the CNT, perpendicular to which only slight deviations from randomness are observed.

Insights into the dynamical behavior can be obtained from the angular orientation autocorrelation times in different spatial regions. In the absence of the CNT all solvents adjacent to the gold surface exhibit significant correlation times of the order of hundreds of ps. The correlation times are significantly increased if the solvents are close to both the CNT and the electrode, except for DMF.

Acknowledgements

Research reported in this publication was supported by the King Abdullah University of Science and Technology (KAUST).

References

1 E. Kamalha, X. Shi, J. I. Mwasiagi and Y. Zeng, *Macromol. Res.*, 2012, **20**, 891–898.
2 M. Sheng, P. Maragakis, C. Papaloukas and E. Kaxiras, *Nano Lett.*, 2007, **7**, 45–50.
3 B. S. Harrison and A. Atala, *Biomaterials*, 2007, **28**, 344–353.
4 C. B. Jacobs, M. J. Peairs and B. J. Venton, *Anal. Chim. Acta*, 2010, **662**, 105–127.
5 S. K. Vashist, D. Zheng, K. Al-Rubeaan, J. H. T. Luong and F.-S. Sheu, *Biotechnol. Adv.*, 2011, **29**, 169–188.
6 A. Star, T.-R. Han, J.-C. P. Gabriel, K. Bradley and G. Grüner, *Nano Lett.*, 2003, **3**, 1421–1423.

7 A. Star, K. Bradley, J.-C. P. Gabriel and G. Grüner, *Prepr. Pap. - Am. Chem. Soc., Div. Fuel Chem.*, 2004, **49**, 887–888.
8 C. Huang, R. K. Wang, B. M. Wong, D. J. McGee, F. Léonard, Y. J. Kim, K. F. Johnson, M. S. Arnold, M. A. Eriksson and P. Gopalan, *ACS Nano*, 2011, **5**, 7767–7774.
9 Y. Zhao, C. Huang, M. Kim, B. M. Wong, F. Léonard, P. Gopalan and M. A. Eriksson, *ACS Appl. Mater. Interfaces*, 2013, **5**, 9355–9361.
10 R. Zangi, *J. Phys.: Condens. Matter*, 2004, **16**, 5371–5388.
11 K. Johnston and V. Harmandaris, *J. Phys. Chem. C*, 2011, **115**, 14707–14717.
12 J. H. Walther, R. Jaffe, T. Halicioglu and P. Koumoutsakos, *J. Phys. Chem. B*, 2001, **105**, 9980–9987.
13 I. Rungger, X. Chen, U. Schwingenschlögl and S. Sanvito, *Phys. Rev. B: Condens. Matter Mater. Phys.*, 2010, **81**, 235407.
14 J. Gao, W. D. Luedtke and U. Landman, *J. Chem. Phys.*, 1997, **106**, 4309–4318.
15 K. Gkionis, I. Rungger, S. Sanvito and U. Schwingenschlögl, *J. Appl. Phys.*, 2012, 112–083714.
16 J. J. Palacios, A. J. Pérez-Jiménez, E. Louis, E. SanFabián and J. A. Vergés, *Phys. Rev. Lett.*, 2003, **90**, 106801.
17 J. C. Phillips, R. Braun, W. Wang, J. Gumbart, E. Tajkhorshid, E. Villa, C. Chipot, R. D. Skeel, L. Kale and K. Schulten, *J. Comput. Chem.*, 2005, **26**, 1781–1802.
18 A. D. MacKerell Jr, D. Bashford, M. Bellott, R. L. Dunbrack Jr, J. Evanseck, M. J. Field, S. Fischer, J. Gao, H. Guo, S. Ha, D. Joseph, L. Kuchnir, K. Kuczera, F. T. K. Lau, C. Mattos, S. Michnick, T. Ngo, D. T. Nguyen, B. Prodhom, I. W. E. Reiher, B. Roux, M. Schlenkrich, J. Smith, R. Stote, J. Straub, M. Watanabe, J. Wiorkiewicz-Kuczera, D. Yin and M. Karplus, *J. Phys. Chem. B*, 1998, **102**, 3586–3616.
19 K. Vanommeslaeghe, E. Hatcher, C. Acharya, S. Kundu, S. Zhong, J. Shim, E. Darian, O. Guvench, P. Lopes, I. Vorobyov and A. D. MacKerell Jr, *J. Comput. Chem.*, 2010, **31**, 671–690.
20 H. Heinz, R. A. Vaia, B. L. Farmer and R. R. Naik, *J. Phys. Chem. C*, 2008, **112**, 17281–17290.
21 M. R. Shirts, D. L. Mobley, J. D. Chidera and V. S. Pande, *J. Phys. Chem. B*, 2007, **111**, 13052–13063.
22 T. A. Darden, D. M. York and L. G. Pedersen, *J. Chem. Phys.*, 1993, **98**, 10089–10092.
23 P. Ewald, *Ann. Phys.*, 1921, **64**, 253–287.
24 G. J. Martyna, D. J. Tobias and M. L. Klein, *J. Chem. Phys.*, 1994, **101**, 4177–4189.
25 S. E. Feller, Y. Zhang, R. W. Pastor and B. R. Brooks, *J. Chem. Phys.*, 1995, **103**, 4613–4621.
26 M. Zäch, M. Heuberger and N. D. Spencer, *Tribol. Ser.*, 2002, **40**, 75–81.
27 J. Kleina and E. Kumacheva, *J. Chem. Phys.*, 1998, **108**, 6996–7009.
28 http://www.chemspider.com, accessed 19/12/12.
29 M. Hermida-Ramón and M. A. Rios, *J. Phys. Chem. A*, 1998, **102**, 2594–2602.
30 R. Vargas, J. Garza, D. A. Dixon and B. P. Hay, *J. Am. Chem. Soc.*, 2000, **122**, 4750–4755.
31 S. Grimme, *Angew. Chem., Int. Ed.*, 2008, **47**, 3430–3434.

